Energy Conversion and Management 77 (2014) 424–431

Contents lists available at ScienceDirect

Energy Conversion and Management

journal homepage: www.elsevier.com/locate/enconman

Computational studies on the effect of geometric parameters on the performance of a solar chimney power plant

Sandeep K. Patel, Deepak Prasad, M. Rafiuddin Ahmed *

Division of Mechanical Engineering, The University of the South Pacific, Suva, Fiji

ARTICLE INFO

Article history:
Received 25 May 2013
Accepted 28 September 2013

Keywords:
Solar chimney power plant
Solar collector
Computational fluid dynamics
Optimization
Air flow characteristics

ABSTRACT

A solar chimney power plant (SCPP) is a renewable-energy power plant that transforms solar energy into electricity. The SCPP consists of three essential elements – solar air collector, chimney tower, and wind turbine(s). The present work is aimed at optimizing the geometry of the major components of the SCPP using a computational fluid dynamics (CFD) software ANSYS-CFX to study and improve the flow characteristics inside the SCPP. The overall chimney height and the collector diameter of the SCPP were kept constant at 10 m and 8 m respectively. The collector inlet opening was varied from 0.05 m to 0.2 m. The collector outlet diameter was also varied from 0.6 m to 1 m. These modified collectors were tested with chimneys of different divergence angles (0°–3°) and also different chimney inlet openings of 0.6 m to 1 m. The diameter of the chimney was also varied from 0.25 m to 0.3 m. Based on the CFX computational results, the best configuration was achieved using the chimney with a divergence angle of 2° and chimney diameter of 0.25 m together with the collector opening of 0.05 m and collector outlet diameter of 1 m. The temperature inside the collector is higher for the lower opening resulting in a higher flow rate and power.

1. Introduction

The increases in oil prices and energy demand combined with recent environmental constraints have rapidly increased the global demand for renewable energy. Solar energy is one of the most promising solutions, especially considering its technological advancements and its growth in the recent years. One of the options that will help meet these demands is the solar chimney power plant (SCPP). The SCPP is a proposed type of renewable-energy power plant that transforms solar energy into electricity.

The SCPP is a low temperature power plant consisting of three essential elements – the collector, the chimney, and the wind turbine(s) [1,2]. The chimney is a long cylindrical structure normally placed in the center of a greenhouse collector which is made out of transparent glass or plastic film [3–6]. The height of the collector increases towards the center where the chimney is placed to guide the hot air up the chimney. Turbine(s) are normally placed at the base of the chimney for power generation. The solar radiation enters the collector and gets absorbed by the ground which heats up the air above it. The hot buoyant air rises up towards the chimney base where a turbine is placed. Suction from the chimney draws in more hot air and the cooler air from outside the collector enters the chimney to replace the hot air through natural convection. Power can be generated round the clock by placing water filled bags under the collector roof and this provides an added advantage of this plant over other solar technologies [6].

The first SCPP prototype was proposed by Schlaich and was built in 1982 in Manzanares, Spain [3,7]. Research works were conducted on the plant and it proved that the SCPP concept is technically viable for power generation [8]. There are normally three methods to study the performance characteristics of a solar chimney power plant: analytical method, numerical method and the method based on similarity theory [9].

The very first theoretical model was developed by Mullet [10] who derived the overall efficiency of the SCPP. According to his model, the overall efficiency of the plant is very low and concludes that the SCPP can be used for large scale power generation. Due to this fact, very few experimental models of SCPP were built and tested and more theoretical and mathematical models have been developed to predict the SCPP performance.

Several analytical investigations have been conducted by Refs. [2,3,5,7,11–16] to predict the performance of a SCPP. Koonsrisuk and Chitsomboon [17] compared theoretical models produced by Refs. [7,12–14,16] to study the accuracy of these theoretical models for the prediction of SCPP performance by studying various plant geometrical parameters and the insolation. They even conducted computational fluid dynamics (CFD) studies to compare the results with these theoretical models. According to the results obtained in their study, it can be said that the theoretical models

* Corresponding author.
E-mail address: ahmed_r@usp.ac.fj (M.R. Ahmed).

0196-8904/$ - see front matter © 2013 Elsevier Ltd. All rights reserved.
http://dx.doi.org/10.1016/j.enconman.2013.09.056

Nomenclature

A	flow area, m^2
h_{total}	total enthalpy, kJ/kg
p	pressure, Pa
$P_{available}$	available power, W
SCPP	solar chimney power plant
S_E	source term in the energy equation, W/m^3
S_M	source term in the momentum equation, N/m^3
T	absolute temperature, K
u	velocity
V	air flow velocity, m/s

Greek Symbols

λ	thermal conductivity, W/mK
ρ	density of air, kg/m^3

Subscripts

i	component i
j	component j

produced by [13,16] compared very well with the CFD results and thus are recommended for the prediction of SCPP performance.

Of late, the use of CFD in studying the flow and the performance of SCPP has increased. This is due to the accurate results and flow visualization offered by CFD software. The first known attempt made to simulate the flow in a SCPP using CFD was conducted by Bernardes et al. [18] in which they performed numerical analysis on the natural convection in a radial solar heater to predict the thermo-hydrodynamic behavior of the device by studying different junction shapes at the collector base.

Kirstein and Backstrom [19] performed numerical analysis to study the flow through a SCPP collector-chimney transition section using commercial CFD software, ANSYS-CFX. CFX was used to verify the experimental data of a scaled model SCPP. Due to the very good agreement between the experimental and numerical results, CFD software can be used to predict the performance of a full sized SCPP.

Further studies using CFD were conducted by Tingzhen et al. [3] and Sangi et al. [20]. Tingzhen et al. [3] performed numerical simulation on the Manzanares SCPP coupled with a three-bladed turbine to validate their CFD code. The CFD code showed good agreement with the experimental data and a MW-grade SCPP was designed and numerically tested with a five bladed turbine to provide a reference for the design of large scale SCPP systems. Sangi et al. [20] developed a mathematical model of a SCPP based on the Navier–Stokes, continuity and energy equations. They also performed numerical simulations using a commercial CFD software FLUENT for the Manzanares SCPP. Both the mathematical model and the numerical analysis were compared to the experimental data and showed a good quantitative agreement.

Koonsrisuk and Chitsomboon [21] studied the effect of tower area change on a SCPP using CFX. From their studies, it can be concluded that divergent tower helps increase the mass flow rate and kinetic energy compared to a constant area tower and the maximum kinetic energy occurs at the tower base. For a convergent tower, the velocity increases at the tower top but the mass flow rate decreases thus causing the kinetic energy to be similar to that of a constant area tower.

A recent study using CFD was conducted by Ming et al. on the influence of ambient crosswind on the performance of a SCPP [22]. According to their study, ambient crosswind has a positive and a negative effect on the performance of a SCPP. When the ambient crosswind is weak, the flow field is deteriorated and the output power reduces. When the ambient crosswind is strong enough, the mass flow rate increases, thus the output power also increases. This increases in mass flow rate results from a wind suction effect on top of the chimney caused by the high velocity wind (Bernoulli principle). Further numerical analysis was conducted by Ming et al. [23] to overcome the negative effect of strong ambient crosswind by employing a blockage a few meters away from the collector inlet opening. According to their study, negative effects resulting from strong ambient crosswinds have been greatly overcome by a large extent with the help of these blockages.

The present work investigates the influence of various geometrical parameters on a fixed solar chimney height and collector diameter to improve the performance of SCPP. Geometric parameters such as collector inlet opening, collector outlet diameter, collector outlet height, chimney inlet opening and chimney divergence angles were varied and tested with different configurations to study and improve the air flow characteristics inside a SCPP.

2. Methodology

ANSYS-CFX Version 14 was used for simulation purpose in this research project. ANSYS-CFX Version 14 uses unsteady Navier–Stokes equation in their conservation form to solve set of equations. The instantaneous equation of mass (continuity), momentum, and energy conservation are presented below [17]:

$$\text{Mass conservation}: \frac{\partial y}{\partial x_i}(\rho u_i) = 0 \tag{1}$$

$$\text{Momentum conservation}: \frac{\partial y}{\partial x_j}(\rho u_i u_j) = -\frac{\partial p}{\partial x_j} + S_M \tag{2}$$

$$\text{Energy conservation}: \frac{\partial y}{\partial x_j}(\rho u_i h_{total}) = -\frac{\partial p}{\partial x_i} + \left(\lambda \frac{\partial T}{\partial x_i}\right) + u_i S_M + S_E \tag{3}$$

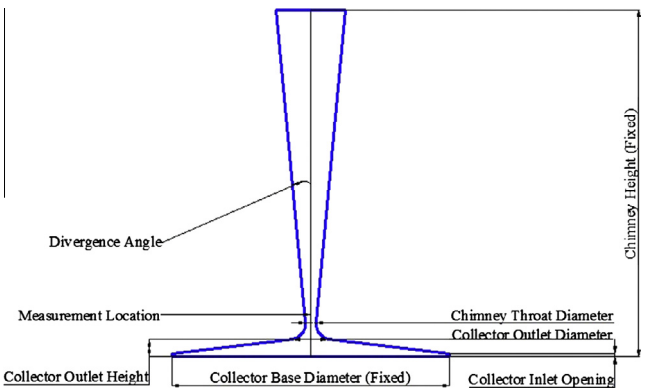

Fig. 1. Diagram of the SCPP with the various parameters that are studied.

2.1. Modeling

The SCPP model was created using Autodesk Inventor software. The solar chimney and the solar air collector were modeled separately for ease of meshing. The model was created on the x–y plane and was revolved around the z-axis to obtain the three-dimensional model. The overall height of the SCPP was 10 m and the solar air collector was 8 m in diameter. The collector inlet height and the chimney divergence angle were varied in this work, as shown in Fig. 1. Different configurations of the SCPP were tested out and are made into cases for ease of understanding as shown in Table 1. The collector base height was varied from 0.5 m, 0.75 m and 1 m from the ground level. The collector outlet diameter was varied from 0.6 m to 1 m and the chimney throat diameter was varied from 0.25 m to 0.3 m, as shown in Table 1. All of these combinations were tested for collector inlet openings of 0.05 m, 0.10 m, 0.15 m and 0.20 m and divergence angles of 0° to 3° in increments of 1°. A total of more than 190 sets with different combinations of the above parameters were studied.

2.2. Meshing

ICEM CFD software was used for grid generation. The computational domain was discretized using the ICEM CFD Hexa-mesher or user-defined meshing method. The hexahedral grid used ensures that the results obtained are of the highest quality and accuracy. Meshing for the solar chimney and solar air collector are shown in Figs. 2 and 3.

A grid independence test was done using three different grid sizes of 10,397, 157,432 and 904,392 nodes respectively. The judging criterion was the mass flow rate. The mass flow rates obtained were 0.159853, 0.469062 and 0.464094 kg/s respectively. The mass flow rate obtained at 157,432 and 904,392 nodes grid size showed very little difference which was of the order of 1%. So having a very fine mesh would not have been beneficial as it would have prolonged the simulation time and for this reason, a grid size of 157,432 nodes was chosen for all the simulations.

2.3. Numerical method

The CFD work in this study was carried out using ANSYS-CFX. ANSYS-CFX is a Reynolds Averaged Navier–Stokes Equation (RANSE) solver based on finite volume technique. For the simulations, steady state analysis was chosen. The computational domain was divided into two which consisted of the solar chimney and the solar air collector. The working fluid used was air which was modeled as an ideal gas. The entire model was built from the origin and extended in the positive y-direction. The buoyancy model was then activated by specifying the gravity of $-g$ in the y-direction which represented real life flow. The reference pressure used was 1 atm. The heat transfer model selected for the current simulation was total energy. This option was chosen because change in kinetic energy is of significant importance in addition to the changes in temperature. The boundary type at the inlet was opening with boundary conditions of zero relative pressure and a static temperature of 303 K. The boundary type at the outlet was also set as opening with a relative pressure of zero and a static temperature of 303 K since the temperature at the height of 10 m does not differ too much compared to the ground air temperature. The ground was assigned a boundary type of wall with no-slip condition activated. The temperature of the ground was set as 323 K. The remaining sides of the computational domain were modeled as wall with no-slip condition. The no-slip condition ensures that the fluid moving over the solid surfaces does not have a velocity relative to the surfaces at the point of contact. Finally, appropriate interface region was created between the chimney and the solar air collector. Automatic mesh connection method was selected for the interface. The simulation was run for 5000 iterations; for convergence, residual type of RMS and the residual target value of 1×10^{-7} were set as the criteria. Fig. 4 shows the boundaries for the SCPP.

3. Results and discussions

The numerical simulation results are presented in this section. The power available for the turbine was calculated using:

$$P_{\text{available}} = 0.5\rho AV^3 \tag{4}$$

The power available was calculated at the measurement location, shown in Fig. 1, where the maximum air velocity was recorded.

Fig. 5 shows the power available for different chimney divergence angles for all collector inlet openings for case 5. The available power was the highest for the 0.05 m opening and lowest for the 0.2 m opening. The peak available power was observed for the divergence angle of 2°. The high values of available power for 0.05 m opening are due to the high values of mass flow rate and velocity compared to other collector openings. The high mass flow rates and velocities are caused by very little interaction of the heated air in the solar air collector with the ambient temperature and this creates a large heating area in the solar air collector; this results in air getting heated up faster and rising through the chimney; consequently more fresh air is drawn into the collector from the opening. For the collector opening of 0.2 m, the air inside the solar air collector interacts more with the ambient air and causing a lesser heating of air in the solar air collector. Similar trends were observed for other cases. According to a study conducted by Serag-Eldin [24], atmospheric winds play a major role in the performance of a SCPP. Strong atmospheric winds result in a total degradation on the performance of a SCPP while weak atmospheric wind also

Table 1
Different configurations of the SCPP tested in the present work.

Cases	Collector outlet height (m)	Collector outlet diameter (m)	Chimney throat diameter (m)
1	0.5	0.6	0.25
2	0.5	0.6	0.3
3	0.5	1	0.25
4	0.5	1	0.3
5	0.75	0.6	0.25
6	0.75	0.6	0.3
7	0.75	1	0.25
8	0.75	1	0.3
9	1	0.6	0.25
10	1	0.6	0.3
11	1	1	0.25
12	1	1	0.3

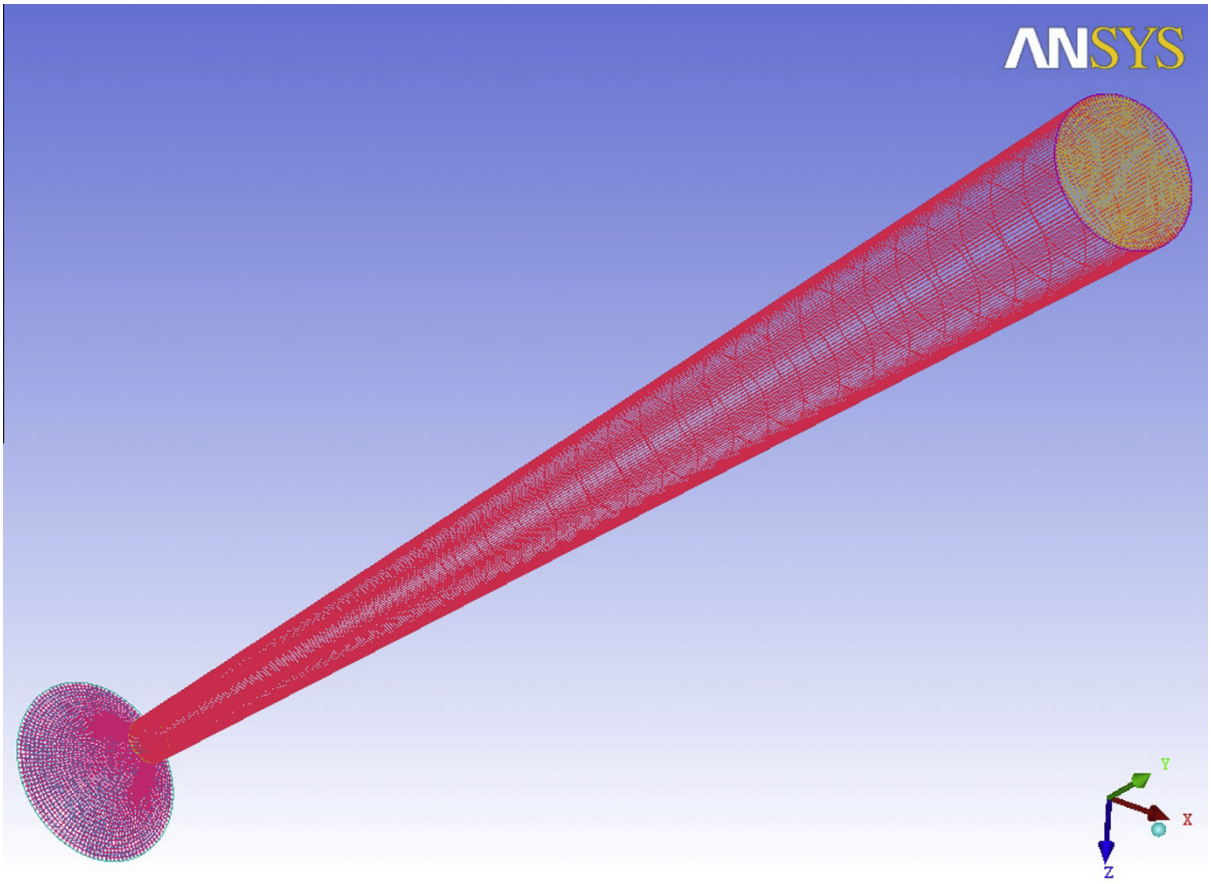

Fig. 2. The meshed solar chimney.

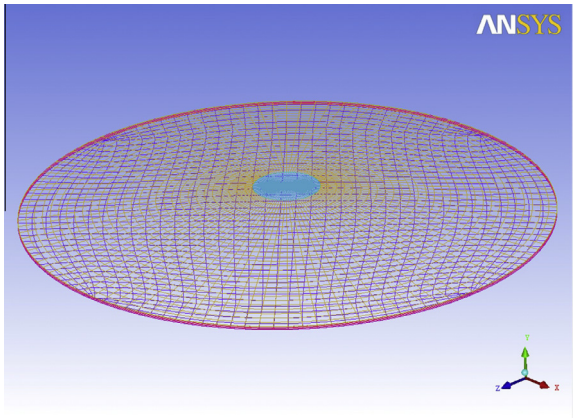

Fig. 3. The meshed solar air collector.

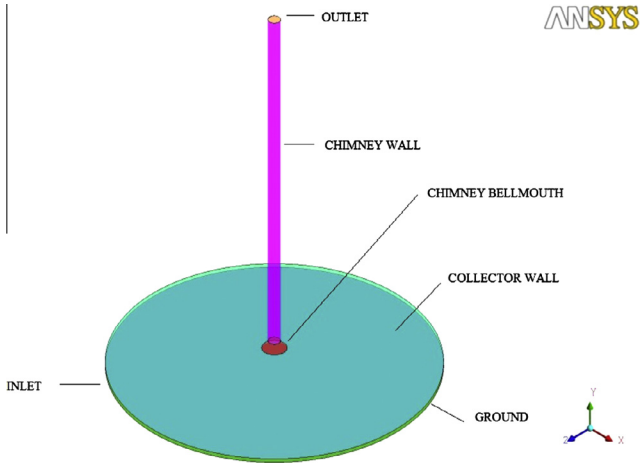

Fig. 4. Various boundaries of the SCPP.

affect the performance of a SCPP unless the collector inlet opening is kept low.

Fig. 6 shows the temperature distribution on the collector for the 0.05 m opening case. It can be seen that the temperature is higher over a large area near the center of the collector. This caused the faster heating up of the air and flow through the chimney, and drawing more fresh air, as described above. Compared to this, when the opening is 0.2 m, the temperature is lower in the same area as the case for Fig. 7. This causes the flow through the chimney to be less compared to the 0.05 m opening case. Hence, the power available for the 0.05 m opening is much higher compared to the 0.2 m opening, as shown in Fig. 5.

Fig. 8 shows the power available for a constant collector inlet opening of 0.1 m at different chimney divergence angles for case 1, case 5 and case 9. The collector outlet diameter is 0.6 m for all the cases. The available power was the highest for case 5 (collector outlet height of 0.75 m) and lowest for case 1 (collector outlet height of 0.5 m). The high values of available power for case 5 are due to the high values of mass flow rate and velocity compared to other collector outlet heights. The low values of available power in case 1 are due to the lower volume of air entering the chimney. When the hot air near the collector opening interacts with the

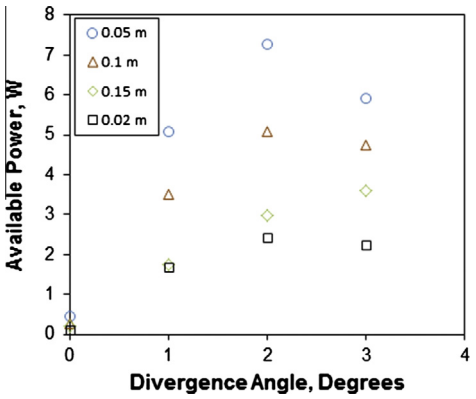

Fig. 5. Power available for case 5 for various collector inlet openings and various chimney divergence angles.

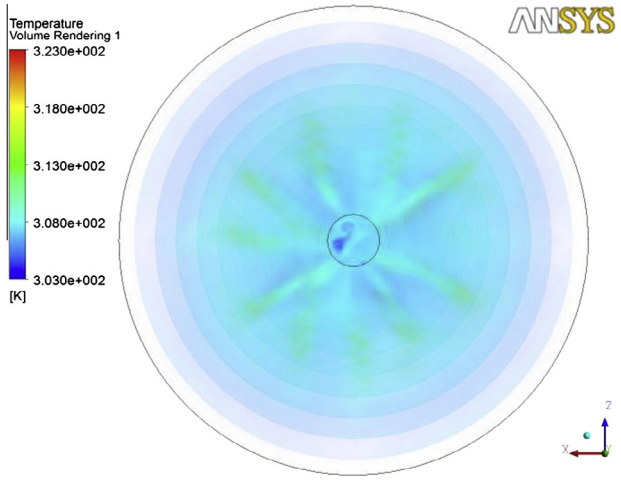

Fig. 6. Temperature contours on the collector for a collector inlet opening of 0.05 m.

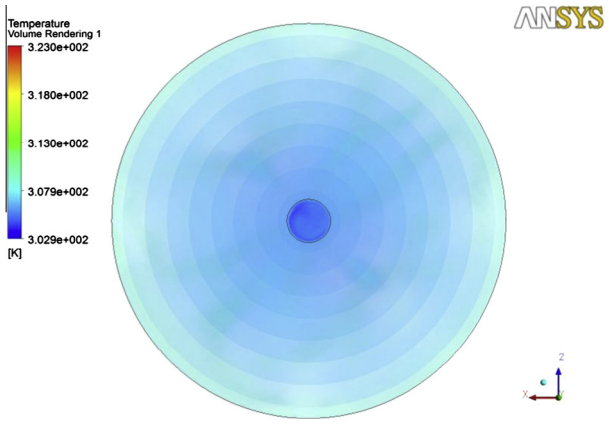

Fig. 7. Temperature contours on the collector for a collector inlet opening of 0.2 m.

ambient air outside the collector due to natural convection taking place, about 1/3 the radius of the collector gets affected by this phenomenon and these causes less air to rise up in the collector entering the chimney. This interaction of the heated air and the ambient air is similar in all the three cases, but for case 5, due to the higher collector outlet height, enough air enters the chimney with less collision between air particles. For case 9, it is similar to case 5 but due to the larger collector outlet height; more

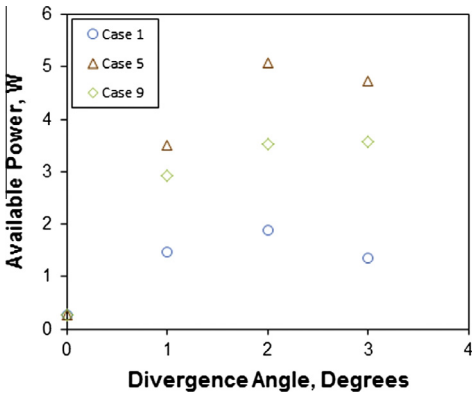

Fig. 8. Power available at different chimney divergence angles for cases 1, 5 and 9 for the collector inlet openings of 0.1 m.

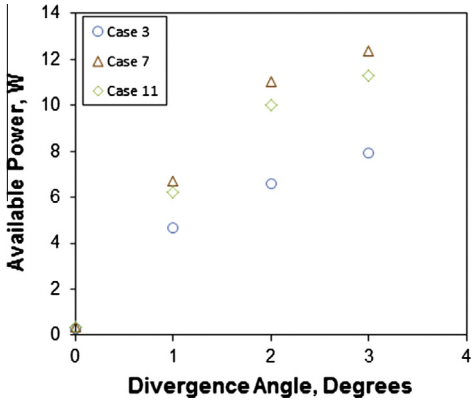

Fig. 9. Power available for cases 3, 7 and 11 for the collector inlet openings of 0.1 m and different chimney divergence angles.

collisions of air particles take place since the chimney inlet diameter is small, thus affecting the overall performance of the SCPP. Similar trends were observed for other cases.

Fig. 9 shows the power available for a constant collector opening of 0.1 m at different chimney divergence angles for case 3, case 7 and case 11. These cases are similar to cases 1, 5, and 9 but with a different collector outlet diameter of 1 m. The available power was the highest for case 7 and lowest for case 3. The high values of available power for case 7 are due to the higher mass flow rates and velocities compared to other collector outlet heights. Also,

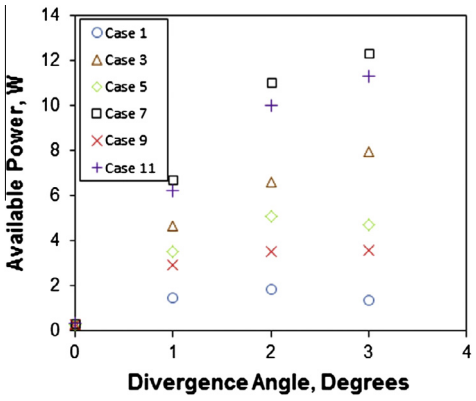

Fig. 10. Power available for cases 1, 3, 5, 7, 9 and 11 for the collector inlet opening of 0.1 m and different chimney divergence angles.

compared to Figs. 8 and 9 has higher available power peaks for all collector outlet heights. The larger collector outlet diameter of 1 m increases the volume of air entering the chimney as the resistance to the flow is less for this case, thus having higher available power. Similar trends were observed for other cases. It can be concluded from Fig. 8 and 9 that the collector outlet diameter is a very important factor in the design of a SCPP and by increasing the collector outlet diameter, the power available will vastly increase due to the higher mass flow rates and velocities. Fig. 10 shows a better representation of cases 1, 3, 5, 7, 9 and 11 combined together for a constant collector opening of 0.1 m at different divergence angles. It is clearly seen that the available power for the collector outlet diameter of 1 m is higher than that of the collector outlet diameter of 0.6 m in all the respective cases.

Fig. 11 shows the power available for a constant collector opening of 0.1 m at different values of chimney divergence angle for case 2, case 6 and case 10. These cases are similar to cases 1, 5, and 9 but with a chimney throat diameter of 0.3 m. The available power is the highest for case 6 and lowest for case 2 showing a similar trend to Fig. 8. The high values of available power for case 6 are due to the high values of mass flow rate and velocity compared to other collector outlet heights. The low values of available power in case 2 are due to the lower volume of air entering the chimney. By comparing Figs. 8 and 11, it can be noted that the overall trends are similar but the magnitude of the power available is different. The higher power available in case 2 compared to case 1 is mainly due to the higher mass flow rate of air entering the chimney. However, for case 5 and case 6, even though the mass flow rate was higher for case 6, the power available was still higher for case 5 due to higher velocity caused by the smaller chimney diameter which acts as a nozzle increasing the velocity of air entering the chimney. Fig. 12 shows a better representation of cases 1, 2, 5, 6, 9 and 10 combined together for a constant collector opening of 0.1 m at different values of chimney divergence angle.

Fig. 13 shows the velocity vectors for case 3 which has the highest available power compared to all other cases. Case 3 had a collector opening of 0.05 m with a collector height of 0.5 m. The collector outlet diameter was 1 m with a chimney diameter of 0.25 m diverging at 2°. The maximum available power for this case is 14.504 W. The maximum velocity achieved is 7.864 m/s and the mass flow rate is 0.469 kg/s. Fig. 14 shows the temperature contours for case 3. The temperature is higher towards the center of the collector. Fig. 15 shows the temperature variation along the chimney for case 3. It can be seen that the temperature generally decreases up to a height of 4 m and slightly increases afterwards. This slight increase in temperature is very small (less than 1 K) and may be due to the friction at the wall of the chimney. An

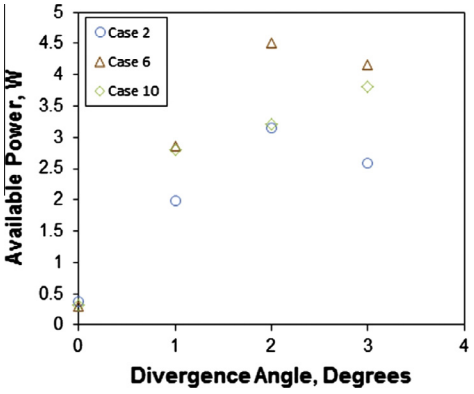

Fig. 11. Power available for cases 2, 6 and 10 for the collector inlet opening of 0.1 m and different chimney divergence angles.

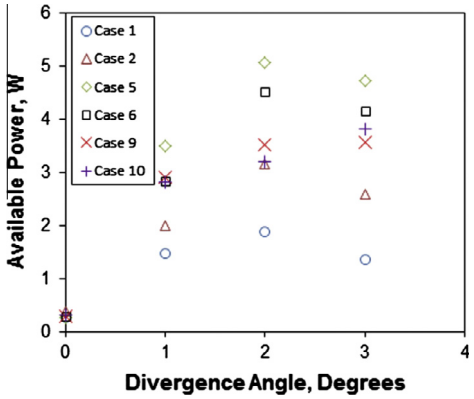

Fig. 12. Power available for cases 1, 2, 5, 6, 9 and 10 for the collector inlet opening of 0.1 m and different chimney divergence angles.

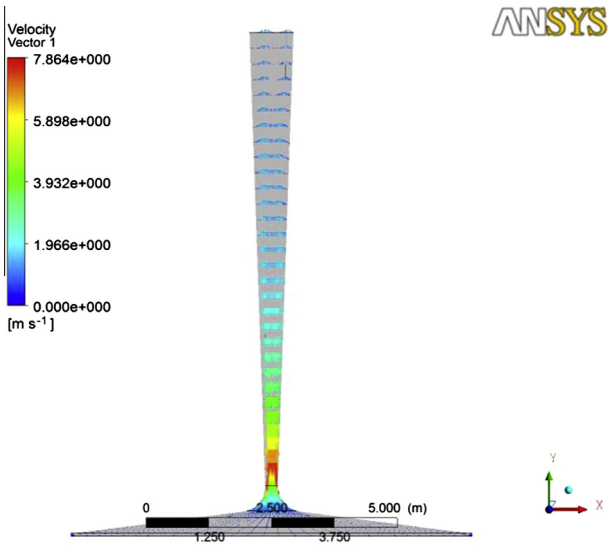

Fig. 13. Velocity vectors on the entire SCPP for case 3 for the collector inlet opening of 0.05 m and chimney divergence angle of 2°.

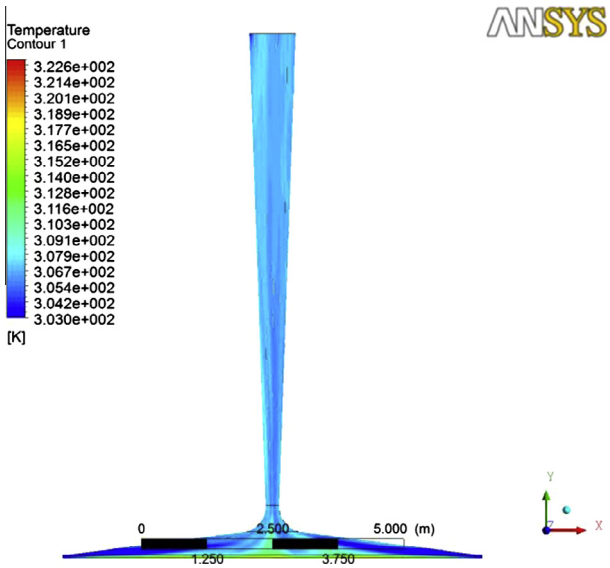

Fig. 14. Temperature contours on the entire SCPP for case 3 for the collector inlet opening of 0.05 m and chimney divergence angle of 2°.

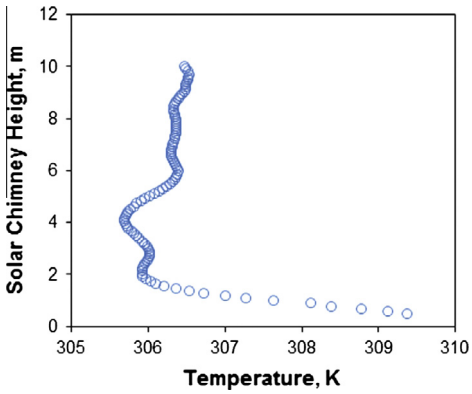

Fig. 15. Temperature variation along the chimney height for case 3 for the collector inlet opening of 0.05 m and chimney divergence angle of 2°.

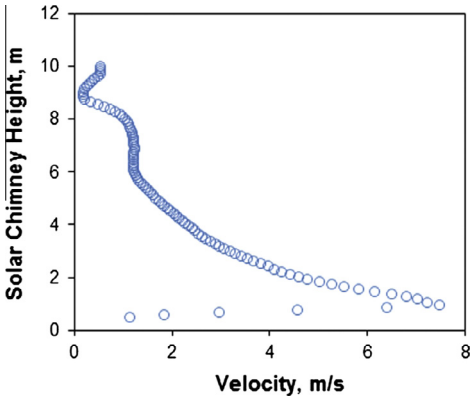

Fig. 16. Velocity variation along the chimney height for case 3 for the collector inlet opening of 0.05 m and chimney divergence angle of 2°.

experimental study conducted by Zhou et al. [25] showed a general decrease in air temperature along the chimney height. The overall temperature variation along the chimney is very similar from the experimental and CFX results.

Fig. 16 shows the velocity variation along the chimney for case 3. The velocity generally increases to a height of 1 m and then decreases afterwards. The increase in velocity is due to the reduction in area (nozzle effect) and decreases due to the diverging duct. Similar trends were also observed by Sangi et al. [20] and Chergui et al. [26] in their study of SCPP.

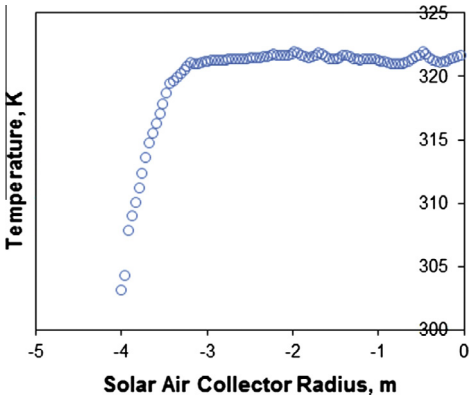

Fig. 17. Temperature variation along the outer radius of the collector to the center measured at 0.025 m above ground for case 3 for the collector inlet opening of 0.05 m and chimney divergence angle of 2°.

Fig. 17 shows the temperature at a height of 0.025 m along the radius of the collector from the outer periphery to the center. The temperature inside the collector increases from the ambient temperature of 303 K at the outer periphery to a temperature of 321 K at about 0.8 m inside the collector. The temperature remains essentially constant away from the collector edges. These trends were very similar to the experimental results obtained by Zhou et al. [25]. The temperature difference was also very similar to that experimental study.

Fig. 18 shows the temperature variation from the base of the collector to the collector outlet at the center of the tower. The temperature decreases as the air rises up towards the chimney. The maximum temperature change inside the collector is 17°. Fig. 19 shows the velocity variation from the base of the collector to the collector outlet at the center of the tower. The velocity increases towards the throat of the chimney. Fig. 20 shows the temperature from the base of the collector to the top of the chimney. The temperature essentially drops although there is a small increase towards the chimney exit. Previous works also reported a drop in temperature towards the chimney outlet. Fig. 21 shows the velocity from the base of the collector to the top of the chimney. The velocity increases till the throat where the maximum velocity is recorded; after which the velocity starts to decrease till close to the chimney outlet, after which there is a small increase in velocity probably due to the temperature difference between the chimney air and the ambient air.

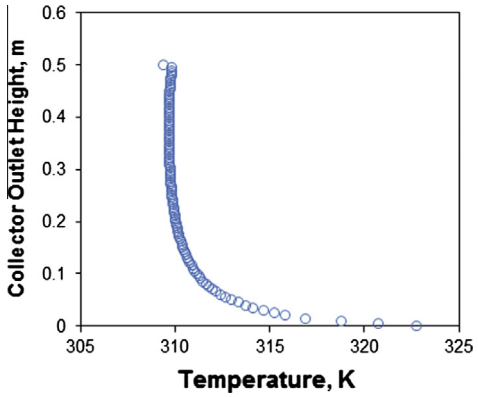

Fig. 18. Temperature variation from the ground to the collector outlet at the center for case 3 for the collector inlet opening of 0.05 m and chimney divergence angle of 2°.

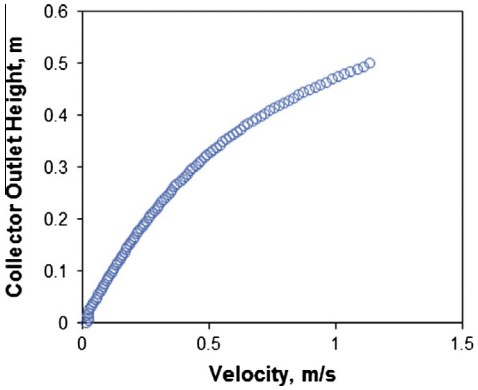

Fig. 19. Velocity variation from the ground to the collector outlet at the center for case 3 for the collector inlet opening of 0.05 m and chimney divergence angle of 2°.

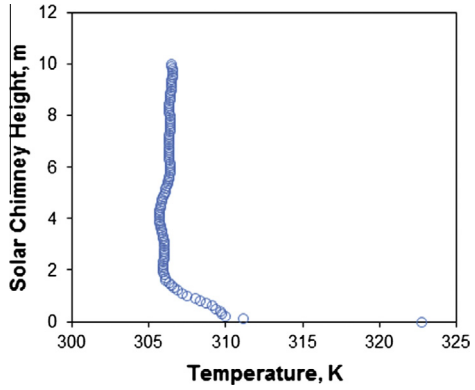

Fig. 20. Temperature variation from the ground to the top of the chimney for case 3 for the collector inlet opening of 0.05 m and chimney divergence angle of 2°.

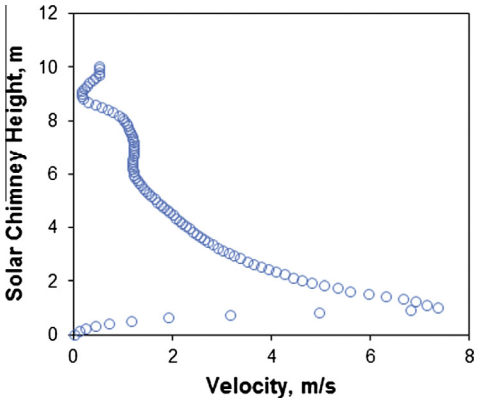

Fig. 21. Velocity variation from the ground to the top of the chimney for case 3 for the collector inlet opening of 0.05 m and chimney divergence angle of 2°.

4. Conclusions and recommendations

The effects of various geometric parameters on a SCPP are presented. It can be concluded that increasing the collector inlet opening significantly influences the overall performance of a SCPP. In the present work, a collector inlet opening of 0.05 m provides the best performance. The collector outlet height is also a very important parameter in the design of a SCPP. The collector outlet should not be too high or too low, but at an optimum height to provide best performance for a SCPP. The collector outlet diameter and the chimney inlet diameter are also important parameters in the design of a SCPP. This determines the amount of air entering the chimney which has a direct relationship to the power available. The divergent chimney is found to perform better than a straight or a converging chimney in terms of mass flow rate and kinetic energy. An optimum divergence angle of 2° was obtained in the present work. The best configuration found from the present work gave a maximum velocity of 7.864 m/s. This work can be extended to different chimney heights and collector diameters and then non-dimensional optimized values can be proposed.

References

[1] Ninic N. Available energy of the air in solar chimneys and the possibility of its ground – level concentration. Sol Energy 2006;80:804–11.
[2] Bernardes MAdS, Vob A, Weinrebe G. Thermal and technical analyses of solar chimneys. Sol Energy 2003;75:511–24.
[3] Tingzhen M, Wei L, Guoling X, Yanbin X, Xuhu G, Yuan P. Numerical simulation of the solar chimney power plant systems coupled with turbine. Renew Energy 2008;33:897–905.
[4] Hamdan MO. Analysis of a solar chimney power plant in the Arabian Gulf region. Renew Energy 2011;36:2593–8.
[5] Pasumarthi N, Sherif SA. Experimental and theoretical performance of a demonstration solar chimney model – Part 1: Mathematical model development. Int J Energy Res 1998;22:277–88.
[6] Mostafa AA, Sedrak MF, Dayem AMA. Performance of a solar chimney under Egyptian weather conditions: numerical simulation and experimental validation. Energy Sci Technol 2011;1:49–63.
[7] Zhou X, Yang J, Xiao B, Hou G, Xing F. Analysis of chimney height for solar chimney power plant. Appl Therm Eng 2009;29:178–85.
[8] Koonsrisuk A, Chitsomboon T. Partial geometric similarity for solar chimney power plant modelling. Sol Energy 2009;83:1611–8.
[9] Petela R. Thermodynamic study of a simplified model of the solar chimney power plant. Sol Energy 2009;83:94–107.
[10] Mullet LB. Solar chimney – overall efficiency. Des Perform Int J Ambient Energy 1987;8:35–40.
[11] Padki MM, Sherif SA. Solar chimney for medium-to-large scale power generation. In: Proceedings of the Manila International Symposium on the Development and Management of Energy Resources. Philippines: Manila; 1989.
[12] Chitsomboon T. A validated analytical model for flow in solar chimney. Int J Renew Energy Eng 2001;3:339–46.
[13] Schlaich J, Bergermann R, Schiel W, Weinrebe G. Design of commercial solar updraft tower systems – utilization of solar induced convective flows for power generation. J Sol Energy Eng 2005;127:117–25.
[14] Tingzhen M, Wei L, Guoliang X. Analytical and numerical investigation of the solar chimney power plant systems. Int J of Energy Res 2006;30:861–73.
[15] Backstrom TWV, Fluri TP. Maximum fluid power condition in solar chimney power plants – an analytical approach. Sol Energy 2006;80:1417–23.
[16] Koonsrisuk A, Chitsomboon T. A single dimensionless variable for solar chimney power plant modelling. Sol Energy 2009;83:2136–43.
[17] Koonsrisuk A, Chitsomboon T. Accuracy of theoretical models in the prediction of solar chimney performance. Sol Energy 2009;83:1764–71.
[18] Bernardes MAdS, Valle RM, Cortez MF-B. Numerical analysis of natural laminar convection in a radial solar heater. Int J Therm Sci 1999;38:42–50.
[19] Kirstein CF, Backstrom TWv. Flow through a solar chimney power plant collector-to-chimney transition section. J Sol Energy Eng 2006;128:317.
[20] Sangi R, Amidour M, Hosseinizadeh B. Modelling and numerical simulation of solar chimney power plants. Sol Energy 2011;85:829–38.
[21] Koonsrisuk A, Chitsomboon T. Effect of tower area change on the potential of solar tower. In: The 2nd Joint International Conference on Sustainable Energy and Environment (SEE 2006). Bangkok (Thailand). 2006. p. 1–6.
[22] Ming T, Wang X, Richter RKd, Liu W, Wu T, Pan Y. Numerical analysis on the influence of ambient crosswind on the performance of solar updraft power plant system. Renew Sustain Energy Rev 2012;16:5567–83.
[23] Ming T, Gui J, Richter RKd, Pan Y, Xu G. Numerical analysis on the solar updraft power plant system with a blockage. Sol Energy 2013.
[24] Serag-Eldin M.A. Computing flow in a solar chimney plant subject to atmospheric winds. In: Heat transfer/fluids engineering summer conference. vol. 2. Charlotte (North Carolina). 2004. p. 1153–62.
[25] Zhou X, Yang J, Xiao B, Hou G. Experimental study of temperature field in a solar chimney power setup. Appl Therm Eng 2007;27:2044–50.
[26] Chergui T, Larbi S, Bouhdjar A. Thermo-hydrodynamic aspect analysis of flows in solar chimney power plants – a case study. Renew Sustain Energy Rev 2010;14:1410–8.